CHEMISTRY OF MATERIALS

ARTICLE

pubs.acs.org/cm

Off-Stoichiometry Effects on the Crystalline and Defect Structure of Hexagonal Manganite $REMnO_3$ Films (RE = Y, Er, Dy)

I. Gélard,[†] N. Jehanathan,[‡] H. Roussel,[†] S. Gariglio,[§] O. I. Lebedev,[‡] G. Van Tendeloo,[‡] and C. Dubourdieu*[,†,∥]

[†]Laboratoire des Matériaux et du Génie Physique, CNRS, Grenoble INP, 3 parvis Louis Néel, 38016 Grenoble, France

[‡]Electron Microscopy for Materials Research, University of Antwerp, Groenenborgerlaan 171, 2020 Antwerpen, Belgium

[§]DPMC, University of Geneva, 24 Quai Ernest Ansermet, 1211 Geneva 4, Switzerland

ABSTRACT: The crystalline and defect structure of epitaxial hexagonal $RE_xMn_yO_3$ (RE = Er, Dy) films with varying cationic composition was investigated by X-ray diffraction and transmission electron microscopy. The films are composed of a strained layer at the interface with the substrate and of a relaxed layer on top of it. The critical thickness is of ∼10 to 25 nm. For Mn-rich films (or RE deficient), an off-stoichiometric composition maintaining the hexagonal $LuMnO_3$-type structure is stabilized over a large range of the RE/Mn ratio (0.72−1.00), with no Mn-rich secondary phases observed. A linear dependence of the out-of-plane lattice parameter with RE/Mn is observed in this range. Out-of-phase boundary (OPB) extended defects are observed in all films and exhibit a local change in stoichiometry. Such a large solubility limit in the RE deficient region points toward the formation of vacancies on the RE site ($RE_xMnO_{3-\delta}$, with $0.72 \leq x < 1$), a phenomenon that is encountered in perovskite manganites such as $La_xMnO_{3-\delta}$ ($x < 1$) and that may strongly impact the physical properties of hexagonal manganites.

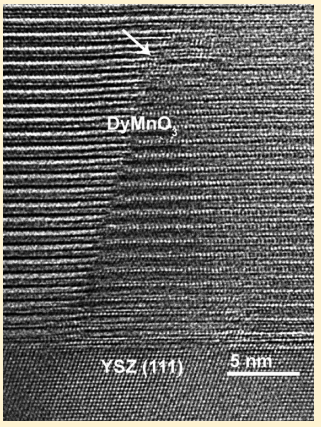

KEYWORDS: hexagonal manganite, multiferroic, MOCVD, stoichiometry, structure, defects

I. INTRODUCTION

Multiferroic compounds have attracted much interest in recent years.[1−4] They exhibit simultaneously at least two ferroic orders in the same phase (or antiferroic orders by extension).[5,6] Besides perovskite-based compounds such as $BiFeO_3$, $BiMnO_3$, orthorhombic rare-earth (RE) manganites (such as $TbMnO_3$) or $RE_2Mn_2O_5$ manganites, hexagonal $REMnO_3$ manganites (RE = Ho−Lu, Y) also display coexistence of ferroelectricity and magnetism. Hexagonal manganites are ferroelectric, with a transition to the paraelectric state in the range 800−1000 K, and also antiferromagnetic, with a transition to the paramagnetic state around 70−100 K. The hexagonal structure can be described as dense oxygen-ion packing (ABCACB) with Mn^{3+} ions having a 5-fold trigonal bipyramidal coordination and with RE^{3+} ions having a 7-fold monocapped octahedral coordination.[7,8] These compounds are of particular interest for their ferroelectric properties, especially as thin films. Their Curie temperature is indeed very high (>900 K) and their polarization is moderate (∼5.5 $\mu C/cm^2$ in bulk $YMnO_3$), which is desirable for applications on silicon substrates to minimize the depolarizing field. They have been considered as gate oxide in field effect transistor for memory applications.[9]

As thin films, the most studied compound is $YMnO_3$.[9−12] The growth of $HoMnO_3$ films[12−16] as well as of hexagonal-stabilized $SmMnO_3$, $GdMnO_3$, $TbMnO_3$, and $DyMnO_3$ films have been also reported.[17−23] However, little is known on the crystalline structure of the films and on their defect chemistry. The role of the composition (cationic and oxygen content) on the structure and on the physical properties of bulk or thin films is hardly evoked in the literature.

Shimura et al. studied the effect of Mn-enrichment in $YMnO_3$ and $YbMnO_3$ ceramics (RE = Y).[24] They showed that excess Mn had a strong impact on leakage currents, dielectric properties, and grain size.[24] The Mn excess was reported to be in a solubility limit within the range of Y(Yb)/Mn ratio 1.0 down to 0.96.[24] For thin films, no detailed study has been reported so far on off-stoichiometric effects. Moreover, large disparities are found in the reported lattice parameters or in the magnetic and ferroelectric properties of such films.

In this paper, we present a detailed study of the effect of the cationic composition on the crystalline structure and related defect structure of epitaxial hexagonal $ErMnO_3$ and $DyMnO_3$ films grown on (111) ZrO_2:Y_2O_3. The relation between film thickness, film composition, and crystalline structure is discussed.

II. EXPERIMENTAL SECTION

$REMnO_3$ (RE = Y, Er, Dy) films were grown on (111) $ZrO_2(Y_2O_3)$ single crystals (a = 0.514 nm), denoted as (111) YSZ. The (111) plane exhibits a reasonable lattice match with the in-plane parameters of the hexagonal $LuMnO_3$-type structure and excellent coincidence of the oxygen atoms at the interface.[18] The synthesis was performed by MOCVD and details are given elsewhere.[25,26] Hexagonal $DyMnO_3$ was obtained

Received: October 11, 2010
Revised: January 5, 2011
Published: February 03, 2011

by epitaxial phase stabilization.[17,18] The substrate temperature was either 850 or 900 °C, the total pressure was 0.66 kPa, and the oxygen partial pressure was 0.33 kPa. After deposition all samples were in situ annealed under 1 atm of O_2 for 15 min at the same temperature as the growth. The thickness effect on the crystalline structure was studied in the range 5 to 500 nm. For each set of films, a same RE/Mn ratio in the precursor solution and a same substrate temperature was used. The compositional effect was studied on $ErMnO_3$ and $DyMnO_3$ films. For both compounds, a set of films with a varying cationic ratio was prepared, which was achieved by varying the RE/Mn ratio in the liquid precursor solution. The $Er_xMn_yO_{3-\delta}$ ($0.72 < Er/Mn < 1.25$) and $Dy_xMn_yO_{3-\delta}$ ($0.63 < Dy/Mn < 1.07$) films thicknesses are 100 and 50 nm, respectively. The cationic composition of the films was determined from wavelength dispersive spectroscopy (WDS) with a ~5% precision. The crystalline structure of the films was studied by X-ray diffraction. $\theta/2\theta$ and φ scans were performed using Cu Kα radiation. Reciprocal space mappings were performed with a high resolution PANalytical X'Pert PRO diffractometer using a two-bounce monochromator for Cu Kα radiation and an asymmetric triple axis analyzer. Selected samples were observed by transmission electron microscopy (TEM) with a JEOL4000EX and FEI Technai G2 microscopes operated at 400 and 200 keV, respectively. Cross-section samples were prepared by mechanical grinding, down to a thickness of about 20 μm, followed by ion-milling. The samples were cut parallel to a cubic plane of the substrate, perpendicular to the contact plane.

III. RESULTS

The $LuMnO_3$-type structure belongs to the $P6_3cm$ space group. Reported values for the c parameter of $YMnO_3$ bulk compound vary from 11.407 Å for single crystals synthesized under Bi_2O_3 flux[27] up to 11.437 Å[28] or 11.441 Å[29] for single crystals grown by the floating zone technique from powders. The a lattice parameter is 6.1387 Å,[27] 6.1469 Å,[28] and 6.146 Å,[29] respectively. The reason for such a large difference in c values is not understood (no experimental evidence was found for Bi atoms incorporation in the crystals grown from Bi_2O_3 flux[28]).

The lattice parameters of bulk $ErMnO_3$ are a = 6.1121 Å and c = 11.42 Å for single crystals grown under Bi_2O_3 flux[30] and a = 6.117 Å and c = 11.455 Å for single crystals grown by the floating zone technique.[29] Bulk hexagonal $DyMnO_3$ was first obtained by high temperature synthesis at 1600 °C followed by a quench.[31] The reported cell parameters for hexagonal $DyMnO_3$ single crystals from the floating zone method are a = 6.189 Å and c = 11.461 Å.[32]

The $YMnO_3$, $ErMnO_3$ and $DyMnO_3$ hexagonal films grow epitaxial on (111) YSZ with the following relationships: $(001)_{hex.}$ $REMnO_3$ // (111) YSZ and $\langle 1\bar{1}0\rangle_{hex.}$ $REMnO_3$ // $\langle 1\bar{1}0\rangle$ YSZ.[33] Nanoinclusions with a secondary orientation were also evidenced by TEM images and second harmonic generation optical measurement[19,33,34] with the following epitaxial relationship to the epitaxial matrix: $(111)_{inclusion}$ $REMnO_3$ // $(001)_{matrix}$ $REMnO_3$ and $\langle 1\bar{1}0\rangle_{inclusion}$ $REMnO_3$ // $\langle 1\bar{1}0\rangle_{matrix}$ $REMnO_3$

A. Film Thickness Effect on Strain Relaxation. In the $\theta/2\theta$ scans performed on films with thickness larger than 25 nm, the 00l peaks are asymmetric, and the asymmetry increases with the film thickness. A clear peak splitting at large angles (008 reflection) is observed for the thickest $ErMnO_3$ and $DyMnO_3$ films. This behavior indicates the presence of at least two out-of-plane lattice parameters and can be attributed to the presence of two layers in the film: a strained (or partially strained) layer at the interface with the substrate (with an out-of-plane parameter noted c_1) and a relaxed (or partially relaxed) layer on top of it (with an out-of-plane parameter noted c_2). Such a two-layer model was proposed for perovskite-type manganite films such as $La_{0.8}MnO_3$[35] or $La_{0.67}Ca_{0.33}MnO_3$ grown on (001) $LaAlO_3$,[36] $La_{0.7}Sr_{0.3}MnO_3$ grown on (001) $SrTiO_3$[37] or the charge-ordered compound $Nd_{0.5}Sr_{0.5}MnO_3$ grown on (001) $LaAlO_3$.[38] It was also reported for other oxides such as $SrRuO_3$ on $SrTiO_3$ (001).[39] The critical thickness for the occurrence of the top relaxed layer is ~25 nm for $YMnO_3$ and $ErMnO_3$ films and ~10 nm for $DyMnO_3$ films. The out-of-plane parameters c_1 and c_2 were calculated from the position of the 008 peaks of the hexagonal manganite; the 222 peak of the YSZ substrate was used as an internal reference. The evolution of the lattice parameters as a function of film thickness is presented in Figure 1. The value corresponding to the bulk compound is indicated for comparison.

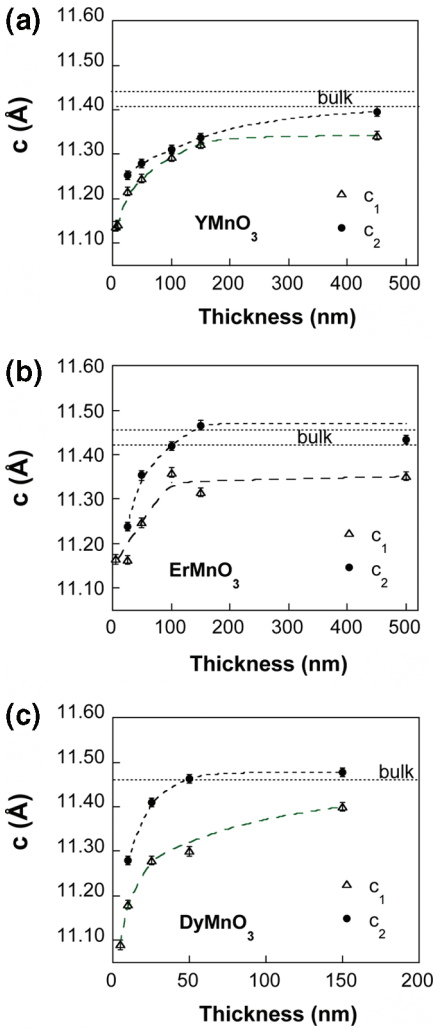

Figure 1. c_1 and c_2 out-of-plane lattice parameters as a function of film thickness for epitaxial hexagonal (a) $YMnO_3$, (b) $ErMnO_3$, and (c) $DyMnO_3$ films on (111) YSZ substrates. Parameters were calculated from the position of the 008 peaks of the manganite films (the 222 peak of the substrate was taken as an internal reference).

A pronounced difference in c_1 and c_2 was observed for all rare-earths (including $TbMnO_3$ and $HoMnO_3$ films not shown here) except for $YMnO_3$. The lattice mismatches at room temperature between substrate and $REMnO_3$ in-plane parameters are 1.7% (Tb), 1.9% (Dy), 2.6% (Ho), 2.7% (Y), and 2.9% (Er). Thus, the relative difference in c_1 and c_2 does not directly correlate with the

dx.doi.org/10.1021/cm1029358 |Chem. Mater. 2011, 23, 1232–1238

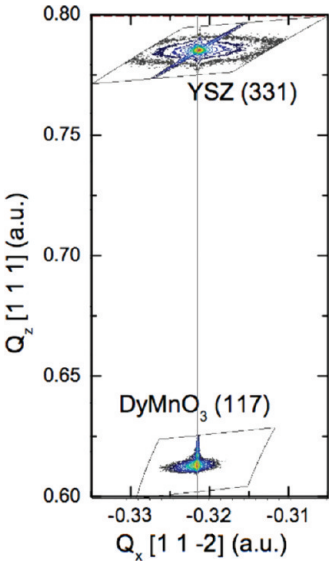

Figure 2. Reciprocal space mapping of 117 reflection for a 50 nm-thick epitaxial $DyMnO_3$ film and of 331 reflection for the YSZ substrate. Axes are labeled according to the YSZ crystalline directions. $DyMnO_3$ film reflections exhibit a single in-plane lattice component.

lattice mismatch. It does not either correlate directly with the ionic radius (the ionic radius of Y^{3+} is comprised between those of $ErMnO_3$ and $HoMnO_3$; $YMnO_3$ exhibits, however, a much less marked difference in c_1 and c_2).

Both c_1 and c_2 increase with film thickness. The strained layer in contact with the substrate exhibits a c_1 parameter smaller than the bulk one. This is in good agreement with in-plane biaxial tensile strain expected from the in-plane lattice mismatch. However, this strained layer is not pseudomorphic with the substrate except for the thinnest films (5 nm or below). The partial relaxation of this layer in contact with the substrate is due to the high temperature postdeposition in situ annealing, which is performed at the same temperature as the growth temperature (850−900 °C). For $DyMnO_3$, which exhibits the lowest lattice mismatch with the substrate, the c_1 value for the 5 nm films (∼ 11.09 Å) is similar to the expected value for a pseudomorphic film (∼ 11.08 Å; this value is calculated assuming an elastic deformation of the cell with an in-plane lattice parameter of $a_{YSZ}(3/2)^{0.5}$ = 6.295 Å and a cell volume of 380.184 $Å^3$). For 5 nm $YMnO_3$ and $ErMnO_3$ films, exhibiting c_1 = 11.13 and 11.16 Å, respectively, the films are already slightly relaxed (the calculated values for pseudomorphic films are ∼10.90 Å and 10.82 Å, respectively).

The out-of-plane c_2 parameter of the top layer is close to the bulk value for the thickest films. $YMnO_3$ full relaxation appears only at thickness of ∼450 nm while c_2 has reached the bulk value at 100 nm for $ErMnO_3$ and 50 nm for $DyMnO_3$. For these two compounds, the c_2 value exceeds the bulk value for thicker films. We also obtained a much larger out-of-plane lattice parameter than the bulk value for $HoMnO_3$ films, for which no saturation of c_2 was observed but a continuous increase with increasing film thickness. A similar result was observed for $HoMnO_3$ films grown by PLD.[40]

The evolution of the in-plane lattice parameter as a function of $YMnO_3$ film thickness was measured by grazing incidence X-ray diffraction. No peak asymmetry was observed, and a single function was used to fit the peak. The a parameter decreases from a = 6.27 Å for the 5 nm-film down to 6.16 Å for 150 nm. The a parameter is larger than the bulk value because of the biaxial tensile strain. Reciprocal space mappings on 117 and 118 reflections were performed on 50, 100, 150, 300, and 450 nm $YMnO_3$ films. The 331 reflection was recorded for the substrate. While the splitting of the 00l peaks was confirmed, no evidence for a multiple in-plane a parameter was found. This result was also confirmed for $DyMnO_3$ films as shown in Figure 2.

There are few crystalline data in the literature for $REMnO_3$ films grown on (111) YSZ substrates and very few studies as a function of film thickness. Moreover, some reported values are rather spread or contradictory. For example, for $YMnO_3$ films, Dho et al.[10] reported a decrease of the c parameter with thickness with an out-of-plane lattice parameter larger than the bulk value for thin films and a leveling off to the bulk value for ∼200 nm thick film, which is in contradiction with expected biaxial tensile strain leading to a compressed c parameter. The in-plane parameter was not reported.

For most studies, the out-of-plane parameter is reported to be lower or similar to the bulk value, (and the a value larger than the bulk value) with the exception of $HoMnO_3$. Kim et al. reported c = 11.6 Å and a = 3.593 Å for a 1 μm thick $HoMnO_3$ film[40] (c_{bulk} = 11.412 Å and a_{bulk} = 3.515 Å for powders[41]). Thus, this film experiences a tensile biaxial strain in the (a,b) plane while the out-of-plane parameter is much larger than the bulk value.

Variation in the c parameter for a same compound and thickness can be due to different deposition conditions associated with different growth methods. However, variations are also observed for a same deposition technique. For instance, parameters of 11.37 Å[14] or 11.45 Å[42] were reported for 100 nm thick $HoMnO_3$ films grown by PLD. Another striking example is the difference that we observed for two sets of hexagonal $YMnO_3$ films prepared by CVD in different precursor solution conditions and at two different temperatures: one grown at 800 °C presented in the ref 12 and another presented here (Figure 1). The parameter c_2 was much larger in the first set[12] (c_2 ∼ 11.45 Å for a 150 nm film). Thus, it appears that both for single crystals and for films, a large variation of the out-of-plane parameter can be observed depending on growth method and conditions. One possible origin may be the cationic and/or oxygen composition that may vary and, with it, the resulting defect chemistry.

B. Effect of the Composition on the Film Structure. The composition of $ErMnO_3$ and $DyMnO_3$ films was varied by varying the precursor solution composition RE/Mn ratio in the range 0.8−1.3, and the resulting hexagonal phase will be noted $RE_xMn_yO_{3-\delta}$. Since the precursors were mixed in a single solution, there was no possible drift of the gas phase RE/Mn composition during deposition. For each compound, the selected thickness for the study (100 nm for $Er_xMn_yO_{3-\delta}$ and 50 nm for $Dy_xMn_yO_{3-\delta}$) corresponds to a bulk-type c_2 value for the series presented in Figure.1. In the CVD process, the cationic film composition is different from the cationic precursor solution composition because of different decomposition yields of the precursors and different metal incorporation yields in the structure. A linear relation is observed between the RE/Mn ratios in the film and precursor solution. The average composition RE/Mn of the films ranges between 0.72−1.25 for $ErMnO_3$ and between 0.63−1.07 for $DyMnO_3$.

For all the studied compositions, the hexagonal phase is observed and only the 00l peaks appear. In the Mn-enriched area (RE/Mn < 1), Mn-rich secondary phase (Mn_3O_4) appears only for Dy/Mn = 0.63. The 008 peaks of the hexagonal phase are split, and their positions change with the cationic composition.

dx.doi.org/10.1021/cm1029358 |*Chem. Mater.* 2011, 23, 1232–1238

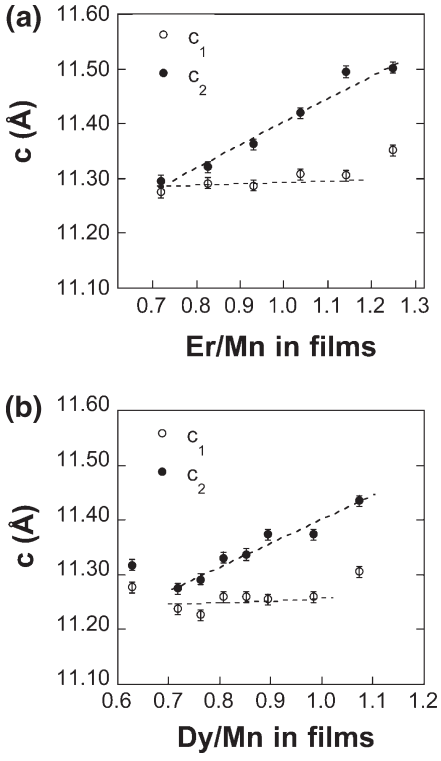

Figure 3. c_1 and c_2 out-of-plane lattice parameters as a function of RE/Mn ratio in the films: (a) 100 nm $ErMnO_3$ films and (b) 50 nm thick $DyMnO_3$ films, all grown at 850 °C on (111) YSZ substrates.

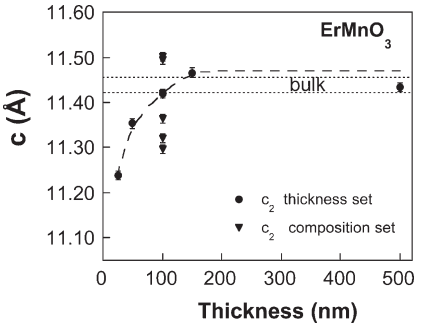

Figure 4. c_2 out-of-plane lattice parameter of $ErMnO_3$ films: results obtained as a function of film thickness and composition are superimposed for comparison.

The evolution of c_1 and c_2 is presented in Figure 3 as a function of RE/Mn ratio in the films.

The parameter c_1 is almost constant for RE/Mn ratios in the range 0.72−1.00 for $Dy_xMn_yO_{3-\delta}$ and 0.72−1.15 for $Er_xMn_yO_{3-\delta}$. This is coherent with the fact that c_1 corresponds to the lattice parameter of the strained layer in direct contact with the substrate, and, as a consequence, the lattice parameters are determined by the substrate lattice rather than the film composition. On the other hand, when the film relaxes, the average film composition has a large effect on the c_2 value with a continuous increase, quasi linear, with increasing RE/Mn ratio. c_2 is smaller than the bulk value when the RE/Mn ratio in the film is inferior to ~1.0. Inversely, c_2 is larger than bulk value when the RE/Mn ratio is superior to ~1.1 (c_2 = 11.49 Å for Er/Mn = 1.15).

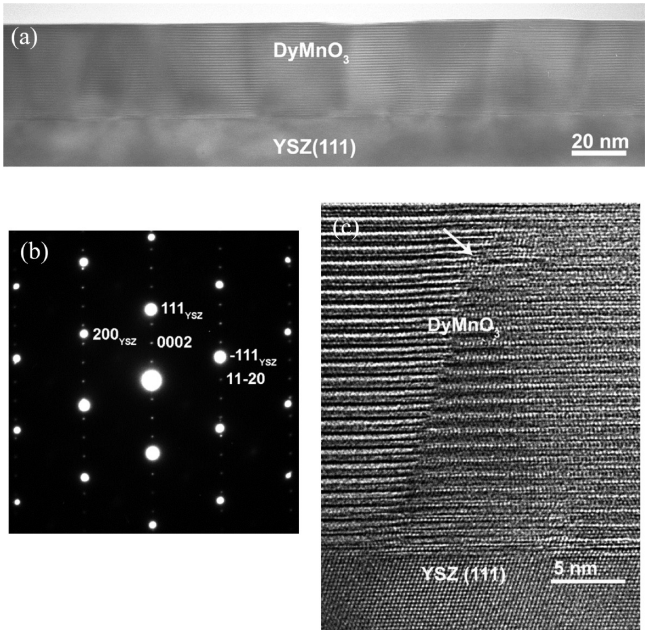

Figure 5. (a) Low magnification TEM image of the $DyMnO_3$ film with Dy/Mn = 0.72; (b) Electron diffraction pattern (ED) of the superposition of the film and substrate in (a); (c) HRTEM image of an out-of-phase boundary (OPB) in the $DyMnO_3$ film with Dy/Mn = 0.89.

This strong dependence of c_2 (which is the main diffraction peak observed for films of 50 nm or thicker) may explain the spread of the out-of-plane lattice parameter values reported in the literature. To illustrate this point, we juxtapose in Figure 4 the results obtained for the evolution of c_2 as a function of film thickness and Er/Mn content.

A set of $Dy_xMn_yO_3$ films with Dy/Mn ratio of 0.72, 0.89, and 1.07 was studied by TEM. Figure 5a shows a low magnification image of a Mn rich (Dy/Mn = 0.72) film. The electron diffraction (ED) pattern shown in Figure 5b is a superposition of film and substrate. The bright reflections correspond to the YSZ substrate; the other reflections are originating from the film and indexed based on a hexagonal structure with $P6_3cm$ space group (185). The epitaxial relationship deduced from the ED patterns for all investigated $Dy_xMn_yO_3$ films ($[0001]_{DyMnO3}$ // $[111]_{YSZ}$ and $(-1100)_{DyMnO3}$ // $(01-1)_{YSZ}$) is consistent with that determined from X-ray diffraction.

Many out-of-phase boundaries (OPB) are observed in these $Dy_xMn_yO_3$ films (Figure 5a,c). These defects are translation boundary defects separating regions that are out of registry by a fraction of the unit cell. The displacement vector (the out-of-phase offset) is ~c/3. They are found to nucleate at the film/substrate interface and generally propagate through the entire thickness of the films while some others appear to have annihilated (leaving a dislocation or joining together in pairs) within the thickness of the film. In agreement with the X-ray diffraction results, TEM studies do not reveal the presence of Mn-rich secondary phases in these films. The excess Mn appears to be distributed within the entire film, but with prominence around the OPB regions (Figure 6). Dy_2O_3 inclusions are observed for the film with a Dy/Mn ratio of 1.07. Figure 7 shows the HR (high resolution) TEM image of such a Dy-rich film. The narrow arrows show the OPBs that originate at the interface region as a result of a substrate surface step (broad arrow). The inset of Figure 7 shows the Fourier transform (FT) from the inclusion,

dx.doi.org/10.1021/cm1029358 |Chem. Mater. 2011, 23, 1232–1238

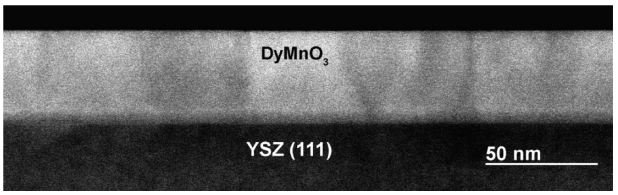

Figure 6. Low magnification high angle annular dark field (HAADF) STEM image of the $DyMnO_3$ film with Dy/Mn = 0.72. The darker regions depict the Mn rich (Dy deficient) areas.

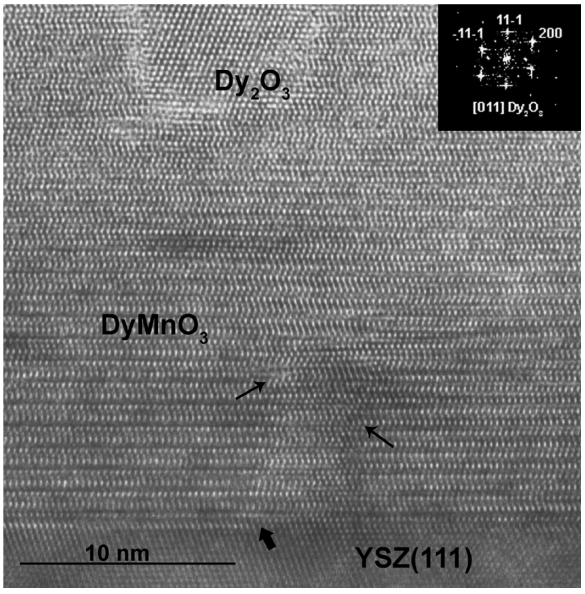

Figure 7. HRTEM image of the $DyMnO_3$ film with Dy/Mn = 1.07. The inset shows the Fourier Transform (FT) of the inclusion. The narrow arrows show the OPBs. The broad arrow shows the surface step at the substrate interface.

which is matched to [011] Dy_2O_3 (a = 0.521 nm; space group $Fm\bar{3}m$ (225)).[43] Er_2O_3 inclusions were also found for the $ErMnO_3$ film with a Er/Mn ratio of 1.04.[33] ED spot splitting (not shown here) is observed from the set of $DyMnO_3$ and $ErMnO_3$ films, indicating a change in the c lattice parameter. This is in agreement with the peak splitting observed from the X-ray diffraction and reciprocal space mapping results.

IV. DISCUSSION

We did not find data in the literature concerning the possible off-stoichiometry solubility limits for these hexagonal $REMnO_3$ phases. In the case of the perovskite $LaMnO_3$ compound, both a large cationic and oxygen off-stoichiometry can exist. $LaMnO_{3+\delta}$ phases (corresponding to $La_{1-\delta}Mn_{1-\delta}O_3$ with equal number of vacancies on A and B sites) have attracted much interest, because of their unusually large range of oxygen non-stoichiometry.[44,45] However, another possible system is the La-deficient manganite $La_{1-x}MnO_{3-\delta}$ one[46,47] ($x > 0$), in which the ratio La/Mn is different from 1. The lanthanum-deficient composition $La_{1-x}MnO_{3-\delta}$ ($x > 0$, $\delta > 0$) can ensure sufficient Mn^{4+} concentration without the formation of vacancies in the Mn sublattice. While $LaMnO_3$ is antiferromagnetic and insulating, $La_{1-x}MnO_{3-\delta}$ phases can exhibit ferromagnetism and metallic conductivity.[46,47] The solubility limit (maximum value of x) depends strongly on the oxygen content. The oxidation can stabilize the perovskite phase in the Mn-enriched area (RE/Mn < 1) owing to an increase in vacancy concentration in the A-sublattice. In bulk $La_{1-x}MnO_{3-\delta}$, the maximum reported value of x is 0.2.[47] For $Nd_{1-x}MnO_{3-\delta}$ ceramics, a single phase is obtained up to x = 0.3−0.4.[49] Thin films of the solid solutions $La_{0.8}MnO_{3-\delta}$ and $Nd_{0.7}MnO_{3-\delta}$ were grown by CVD and similar solubility limits were observed than in the bulk.[35,48,49]

In the case of the hexagonal $REMnO_3$ structure, a cationic off-stoichiometry can also be envisaged with vacancies on the RE and/or Mn sites. Vacancies were proposed for the origin of the large variations of $YMnO_3$ single crystals prepared either under Bi_2O_3 flux or by the floating zone technique.[28] Our study, combining average measurements by X-ray diffraction and local observations by TEM, shows that the hexagonal phase of crystalline $LuMnO_3$-type in the Mn-enriched area (RE/Mn < 1) is stabilized for RE/Mn values as low as 0.72 with no secondary phases. Such a high solubility limit points toward the formation of vacancies on the RE site, with a resulting formula $RE_{1-x}MnO_{3-\delta}$.

In the $LaMnO_3$ system, the change in stoichiometry is accompanied by a distortion of the perovskite structure (orthorhombic or rhomboedral). Overton et al[50] reported a change in symmetry in hexagonal $YMnO_{3-x}$ with a small change in oxygen stoichiometry. They also attributed it to structural disorder, which resulted from the loss in oxide ions. However, in the hexagonal $REMnO_3$ films, no change of the crystalline symmetry was detected. But the OPBs in these films and inclusions (for RE/Mn >1) conform to the compositional fluctuations and non-stoichiometry of the constituent cations.[51,52] It has been reported that extended defects can contribute toward the accommodation of excessive strain energy in epitaxial films, particularly in layered oxides.[51,52] The excess tensile strain in films greater than their critical thickness t_c can be compensated by the compressive strain claimed[52,53] to be present at the structurally shifted domain boundaries (OPBs). The decrease of the RE/Mn ratio from 1 down to 0.72 is accompanied by a linear decrease of the c_2 out-of-plane parameter of the top relaxed layer. The following picture can be proposed. During the growth, a strained layer is formed at the interface with the substrate and the lattice parameters are determined by the substrate parameters. Above a critical thickness t_c, which depends on the rare-earth ($ErMnO_3$ and $YMnO_3$: $t_c \sim 25$ nm, $DyMnO_3$: $t_c \sim 10$ nm), the strain relaxation related to lattice parameters mismatch and off-stoichiometry is accommodated by a change in the out-of-plane parameter of the hexagonal structure. No significant change of the in-plane parameters is observed. The increase in Mn^{4+} concentration (RE deficient films) relatively to the nominal Mn^{3+} valence may contribute to the significant decrease in c_2. OPBs may also contribute to the degree of peak splitting;[51] however, no direct correlation was found between the density of OPBs defects and the film composition.

The presence of vacancies on RE sites, the change in Mn valence, and the OPBs defects should have a significant impact on properties such as leakage current, ferroelectric polarization, or magnetic ordering temperature. The ferroelectricity in $YMnO_3$ has been shown to result from the buckling of the MnO_5 polyhedra accompanied by displacements of the Y ions.[54] Therefore, vacancies on Y sites and the resulting change in the crystalline structure should impact the ferroelectric behavior. The antiferro-magnetically ordered structure can be impacted by the change in Mn valence. Overton et al. showed that the

magnetic behavior of the Mn ions could be tuned by electronic doping via the anion vacancy concentration.[50] We think that cation vacancies could as well affect the magnetic properties. One can note that the literature shows a large spread of T_N values for a same compound. For bulk $YMnO_3$ T_N is reported between ~70 K[55] and ~80 K.[56] For bulk $HoMnO_3$, both T_N and T_{SR} (temperature at which the reorientation of the moments by 90° occurs in the basal plane) reported values are also spread by several degrees (ref 57 and references therein).

These results clearly show that increased attention should be given to off-stoichiometry effects for the understanding of the physical properties of hexagonal manganite films.

V. CONCLUSION

Off-stoichiometry effects on the hexagonal crystalline structure of $REMnO_3$ films (RE = Er, Dy) were investigated. All films contain a significant amount of out-of-phase boundaries with local change in composition. For RE-rich films (RE/Mn > 1), secondary phases of RE_2O_3 or REO_2 are formed. In contrast, in the Mn-enriched area, a solubility limit of RE/Mn ~ 0.72 is found, pointing to the formation of vacancies on the RE site. The decrease of the RE/Mn ratio from 1 down to 0.72 is accompanied by a linear decrease of the out-of-plane lattice parameter of the top relaxed layer of the films. The large solubility limit that allows to crystallize the hexagonal phase without any secondary phases highlights the possible important role of the cationic composition on the physical properties of hexagonal $REMnO_3$ films, whereas off-stoichiometry effects have been so far neglected.

AUTHOR INFORMATION

Corresponding Author

*E-mail: catherine.dubourdieu@grenoble-inp.fr.

Present Address

[||]IBM T.J. Watson Research Center, Yorktown Heights, U.S.A.

ACKNOWLEDGMENT

This study was performed at LMGP in the framework of the European Specific Targeted Research Project MaCoMuFi "Manipulating the Coupling in Multiferroic Films" (No. NMP3-CT-2006-033221). CrysTec (Germany) and SAFC Hitech (U.K.) are acknowledged for providing the substrates and the CVD precursors, respectively. The authors acknowledge financial support from the European Union under the Framework 6 program under a contract for an Integrated Infrastructure Initiative (Reference 026019 ESTEEM).

REFERENCES

(1) Fiebig, M. *J. Phys. D* **2005**, *38*, R123.
(2) Spaldin, N. A.; Fiebig, M. *Science* **2005**, *309*, 391.
(3) Prellier, W.; Singh, M. P.; Murugavel, P. *J. Phys. Cond. Matter* **2005**, *17*, R803.
(4) Eerenstein, W.; Mathur, N. D.; Scott, J. F. *Nature* **2006**, *442*, 759.
(5) Schmid, H. *Ferroelectrics* **1994**, *162*, 317.
(6) Schmid, H. *Ferroelectrics* **2001**, *252*, 41.
(7) Bertaut, F.; Forrat, F.; Fang, P. *C. R. Acad. Sci.* **1963**, *256*, 1958.
(8) Yakel, H. L.; Koehler, W. C.; Bertaut, E. F.; Forrat, E. F. *Acta Crystallogr.* **1963**, *16*, 957.
(9) Fujimura, N.; Azuma, S.-I.; Aoki, N.; Toshimura, T.; Ito, T. *J. Appl. Phys.* **1996**, *80*, 7084.
(10) Dho, J.; Leung, C. W.; MacManus-Driscoll, J. L.; Blamire, M. G. *J. Cryst. Growth* **2004**, *267*, 548.
(11) Marti, X.; Sanchez, F.; Hrabovsky, D.; Fontcuberta, J.; Laukhin, V.; Skumryev, V.; Garcia-Cuenca, M. V.; Ferrater, C.; Varela, M.; Lüders, U.; Bobo, J. F.; Estradé, S.; Arbiol, J.; Peiro, F. *J. Cryst. Growth* **2007**, *299*, 288.
(12) Dubourdieu, C.; Huot, G.; Gélard, I.; Roussel, H.; Lebedev, O. I.; Van Tendeloo, G. *Philos. Mag. Lett.* **2007**, *87*, 203.
(13) Dörr, K.; Thiele, C.; Kim, J.-W.; Bilani, O.; Nenkov, K.; Schultz, L. *Philos. Mag. Lett.* **2007**, *87*, 269.
(14) Murugavel, P.; Lee, J. H.; Lee, D.; Noh, T. W.; Jo, Y.; Jung, M. H.; Oh, Y. S.; Kim, K. H. *Appl. Phys. Lett.* **2007**, *90*, 142902.
(15) Han, T.-C.; Lin, J. G. *IEEE Trans. Magn.* **2008**, *44*, 2930.
(16) Kang, D. H.; Chae, J. H.; Kim, E. S. *J. Electroceram.* **2008**, *21*, 831.
(17) Bosak, A. A.; Dubourdieu, C.; Sénateur, J.-P.; Gorbenko, O.Yu.; Kaul, A.R. *J. Mater. Chem.* **2002**, *12*, 800.
(18) Bosak, A. A.; Dubourdieu, C.; Sénateur, J.-P.; Gorbenko, O.Yu.; Kaul, A. R. *Cryst. Eng.* **2002**, *5*, 355.
(19) Graboy, I. E.; Bosak, A. A.; Gorbenko, O.Yu.; Kaul, A. R.; Dubourdieu, C.; Sénateur, J.-P.; Svetchnikov, V. L.; Zandbergen, H. W. *Chem. Mater.* **2003**, *15*, 2632.
(20) Balasubramanian, K. R.; Bagal, A. A.; Castillo, O.; Francis, A. J.; Salvador, P. A. *Advanced Dielectric, Piezoelectric, and Ferroelectric Thin Films*; Tuttle, B. A., Chen, C., Jia, Q., Ramesh, R., Eds.; Wiley-American Ceramic Society: Indianapolis, IN, 2004; Ceramic Transactions, Vol. 162, p 59.
(21) Balasubramanian, K. R.; Havelia, S.; Salvador, P. A.; Zheng, H.; Mitchell, J. F. *Appl. Phys. Lett.* **2007**, *91*, 232901.
(22) Lee, J.-H.; Murugavel, P.; Lee, D.; Noh, T. W.; Jo, Y.; Jung, M.-H.; Jang, K. H.; Park, J.-G. *Appl. Phys. Lett.* **2007**, *90*, 012903.
(23) Lee, D.; Lee, J.-H.; Murugavel, P.; Jang, S. Y.; Noh, T. W.; Jo, Y.; Jung, M.-H.; Ko, Y.-D.; Chung, J.-S. *Appl. Phys. Lett.* **2007**, *90*, 182504.
(24) Shimura, T.; Fujimura, N.; Yamamori, S.; Yoshimura, T.; Ito, T. *Jpn. J. Appl. Phys.* **1998**, *37*, 5280.
(25) Sénateur, J. P.; Dubourdieu, C.; Weiss, F.; Rosina, M.; Abrutis, A. *Adv. Mater. Opt. Electron.* **2000**, *10*, 155.
(26) Dubourdieu, C.; Gélard, I.; Salicio, O.; Saint-Girons, G.; Vilquin, B.; Hollinger, G. *Int. J. Nanotechnol.* **2010**, *7* (4−8), 320.
(27) Van Aken, B. B.; Meetsma, A.; Palstra, T. T. M. *Acta Crystallogr.* **2001**, *C57* (pt. 3), 230.
(28) Nénert, G.; Pollet, M.; Marinel, S.; Blake, G. R.; Meetsma, A.; Palstra, T. M. *J. Phys.: Condens. Matter* **2007**, *19*, 466212.
(29) Zhou, J.-S.; Goodenough, J. B.; Gallardo-Amores, J. M.; Moran, E.; Alario-Franco, M. A.; Caudillo, R. *Phys. Rev. B* **2006**, *74*, 014422.
(30) Van Aken, B. B.; Meetsma, A.; Palstra, T. T. M. *Acta Crystallogr.* **2001**, *E57* (pt. 6), i38.
(31) Szabo, G.; Paris, R. *C. R. Scéances Acad. Sci., Ser. C* **1969**, *268*, 513.
(32) Harikrishnan, S.; Rossler, S.; Naveen Kumar, C. M.; Bhat, H. L.; Rossler, U. K.; Wirth, S.; Steglich, F.; Suja, E. *J. Phys.: Condens. Matter* **2009**, *21*, 096002.
(33) Jehanathan, N.; Lebedev, O.; Gélard, I.; Dubourdieu, C.; Van Tendeloo, G. *Nanotechnology* **2010**, *21*, 075705.
(34) Kordel, T.; Wehrenfennig, C.; Meier, D.; Lottermoser, Th.; Fiebig, M.; Gélard, I.; Dubourdieu, C.; Kim, J.-W.; Schultz, L.; Dörr, K. *Phys. Rev. B* **2009**, *80*, 045409.
(35) Qian, Q.; Tyson, T. A.; Dubourdieu, C.; Bossak, A.; Sénateur, J. P.; Deleon, M.; Bai, J.; Bonfait, G. *Appl. Phys. Lett.* **2002**, *80*, 2663.
(36) Petit, M.; Rajeswari, M.; Biswas, A.; Greene, R. L.; Venkatesan, T.; Martinez-Miranda, L. J. *J. Appl. Phys.* **2005**, *97*, 093512.
(37) Ranno, L.; Llobet, A.; Tiron, R.; Favre-Nicolin, E. *Appl. Surf. Sci.* **2002**, *188*, 170.
(38) Prellier, W.; Biswas, A.; Rajeswari, M.; Vankatesan, T.; Greene, R. L. *Appl. Phys. Lett.* **1999**, *75*, 397.
(39) Oh Sang, H.; Park, C. G. *J. Appl. Phys.* **2004**, *95*, 4691.
(40) Kim, J.-W.; Nenkov, K.; Schultz, L.; Dörr, K. *J. Magn. Magn. Mater.* **2009**, *321*, 1727.
(41) Munoz, A.; Alonso, J. A.; Martinez-Lope, M. J.; Casais, M. T.; Martinez, J. L.; Fernandez-Diaz, M. T. *Chem. Mater.* **2001**, *13*, 1497.

(42) Kim, J.-W.; Dörr, K.; Kwon, A. R.; Schultz, L. *J. Magn. Magn. Mater.* **2007**, *310*, e352.
(43) Kashaev, A. A.; Ushchapovskii, L. V.; Il'in, A. G. *Soviet Phys.: Crystallogr. (English translation)* **1975**, *20* (1), 114.
(44) Van Roosmalen, J. A. M.; Cordfunke, E. H. P.; Helmholdt, R. B. *J. Solid State Chem.* **1994**, *110*, 100. Van Roosmalen, J. A. M.; Cordfunke, E. H. P. *J. Solid State Chem.* **1994**, *110*, 106. Van Roosmalen, J. A. M.; Cordfunke, E. H. P. *J. Solid State Chem.* **1994**, *110*, 109. Van Roosmalen, J. A. M.; Cordfunke, E. H. P. *J. Solid State Chem.* **1994**, *110*, 113.
(45) Tofield, B. C.; Scott, W. R. *J. Solid State Chem.* **1974**, *10*, 183.
(46) Töpfer, J.; Goodenough, J. B. *J. Solid State Chem.* **1997**, *130*, 117.
(47) Arulraj, A.; Mahesh, R.; Subbanna, G. N.; Mahendiran, R.; Raychaudhuri, A. K.; Rao, C. N. R. *J. Solid State Chem.* **1996**, *127*, 87.
(48) Bosak, A.; Dubourdieu, C.; Audier, M.; Sénateur, J. P.; Pierre, J. *Appl. Phys. A: Mater. Sci. Process.* **2004**, *79*, 1979.
(49) Bosak, A. A.; Gorbenko, O. Yu.; Kaul, A. R.; Graboy, I. E.; Dubourdieu, C.; Sénateur, J. P.; Zandbergen, H. W. *J. Magn. Magn. Mater.* **2000**, *211*, 61.
(50) Overton, A. J.; Best, J. L.; Saratovsky, I.; Hayward, M. A. *Chem. Mater.* **2009**, *21*, 4940.
(51) Zurbuchen, M. A.; Tian, W.; Pan, X. Q.; Fong, D.; Streiffer, S. K.; Hawley, M. E.; Lettieri, J.; Jia, Y.; Asayama, G.; Fulk, S. J.; Comstock, D. J.; Knapp, S.; Carim, A. H.; Schlom, D. G. *J. Mater. Res.* **2007**, *22*, 1439.
(52) Balakrishnan, K.; Arora, S. K.; Shvets, I. V. *J. Phys.: Condens. Matter* **2004**, *16*, 5387.
(53) Koch, R.; Winau, D.; Rieder, K. H. *Phys. Scr.* **1993**, *T49*, 539.
(54) Van Aken, B. B.; Palstra, T. T. M.; Filippetti, A.; Spladin, N. A. *Nat. Mater.* **2004**, *3*, 164.
(55) Munoz, A.; Alonso, J. A.; Martinez-Lope, M. J.; Casais, M. T.; Martinez, J. L.; Fernandez-Diaz, M. T. *Phys. Rev. B* **2000**, *62*, 9498.
(56) Park, J.; Kong, U.; Pirogov, A.; Choi, S. I.; Park, J.-G.; Choi, Y. N.; Lee, C.; Jo, W. *Appl. Phys. A: Mater. Sci. Process.* **2002**, *74*, S796.
(57) Gélard, I.; Dubourdieu, C.; Pailhès, S.; Petit, S.; Simon Ch. *Appl. Phys. Lett.* **2008**, *92*, 232506.

■ NOTE ADDED AFTER ASAP PUBLICATION

There was a minor text error in the abstract in the version published ASAP February 3, 2011; the corrected version published ASAP February 4, 2011.